Supporting Information

Facet-Regulated Oxidative Dehydrogenation of Lactic Acid to Pyruvic Acid on α-Fe_2O_3

Chunyu Yin,[a] Xinli Li,*[a] Yunsheng Dai,[b] Zhi Chen,[a] Dingfeng Yang,[a] Ruixue Liu,[a] Weixin Zou,[c] Congming Tang *[a] and Lin Dong [c]

a. School of Chemistry and Chemical Engineering, Chongqing University of Technology, Chongqing 400054, PR China

b. Catalysis, Sino-Platinum Metals Co., Ltd., Kunming 650106, PR China

c. Jiangsu Key Laboratory of Vehicle Emissions Control, Center of Modern Analysis, Nanjing University, Nanjing 210093, PR China

Experimental Procedures

Materials

All chemicals and solvents were purchased from Micxy Chemical Reagent Co., Ltd and used as received unless otherwise noted. Deionized water (18.2 MΩ cm) was prepared by Pure Water System (GWA-UN) and used throughout experiment.

Synthesis

Hematite α-Fe_2O_3-RC was synthesized by hydrothermal method under alkaline conditions, followed by calcination in air. In a representative experiment to prepare RC, 10 mmol of $Fe(NO_3)_3{\cdot}9H_2O$ and 36 mmol of $CO(NH_2)_2$ were dissolved in 60 mL of deionized water and stirred at room temperature for 30 min. Next, the resultant solution was transferred to 100 mL of PTFE-lined stainless steel hydrothermal reactor, placed in an oven, and kept at 120 °C for 8 h. Then the precipitate was formed, and washed several times with deionized water and absolute ethanol, and dried at 50 °C for 3 h. Catalysts were calcined at 500 °C in air for 3 hours prior to oxidative dehydrogenation of LA to PA and catalyst characterization.

In the previous work, the synthesis method of ferrite nanoparticles for preparation of truncated hexagonal bipyramid, pseudo-cubic and hexagonal plate was described[1]. $K_4[Fe(CN)_6]{\cdot}3H_2O$ (0.337 g) was dissolved in 40.0 mL of a sodium carboxymethyl cellulose (CMC, 300–800 MPa s, 1.25 g L^{-1}) solution; then 0.500 g polyvinyl pyrrolidone (PVP-K30) and 0.30 mL hydrazine hydrate solution ($N_2H_4{\cdot}H_2O$, 80%) were added under ultrasonic treatment until complete dissolution of PVP. The mixture was added into a Teflon-lined stainless steel autoclave (60 mL) and hydrothermally treated at 160 °C for 6 h. After the hydrothermal reaction, the suspension was centrifuged, the solids were washed four times with deionized water and once with ethanol, dried at 80 °C for 5 h, and calcined in air at 300 °C for 3 h. The sample was named as α-Fe_2O_3-THB. The mass of $K_4[Fe(CN)_6]{\cdot}3H_2O$ and hydrazine hydrate solution were changed to 0.253g and 0.90 mL respectively. The other preparation processes are similar to those for the preparation of α-Fe_2O_3-THB. The sample was named as α-Fe_2O_3-QC.

The synthesis of hematite hexagonal nanoplates was based on the previous work[2]. Briefly, 1.092 g of $FeCl_3{\cdot}6H_2O$ was dissolved under vigorously stirring in 40 mL with 2.8 mL deionized water. Afterwards, 3.2 g of sodium acetate was added upon stirring. The mixture was then sealed in a Teflon-lined stainless steel autoclave (60 mL) and hydrothermally treated at 180 °C for 7 h. Upon cooling to room temperature, the other separation and washing procedures are similar to those for the preparation of α-Fe_2O_3-THB. The sample was named as α-Fe_2O_3-HS.

Activity evaluation

The vapor phase oxidative dehydrogenation of LA to PA was carried out with a continuous up-down fixed-bed quartz tubular reactor (4 mm inner diameter) at atmospheric pressure. The catalyst (ca. 0.30 g, 20-40 meshes) was placed between two layers of quartz wools inside reactor. Firstly, the catalyst was heated from room temperature to 230 °C at a rate of 5 °C min^{-1}, and maintained at the temperature for 0.5 h by following air (3.0 mL min^{-1}). Then the feedstock (10 wt% aqueous solution of LA, 2.0 mL h^{-1}) was pumped into the reactor and driven through the catalyst bed by air (0.1 MPa, 3.0 mL min^{-1}). The contact time of reactant over the catalyst was evaluated to obtain around 0.30 s with equation (1) according to previous references[3, 4]. The liquid products were analyzed off-line using a SP-6890 gas chromatograph with a FFAP capillary column connected to a FID for acetic acid and acetaldehyde, and LC-20AD liquid chromatograph with a reversed-phase C18 column connected to a UV detector for lactic acid, pyruvic acid and acrylic acid. GC-MS analyses of the samples were performed using Agilent 5973N Mass Selective Detector attachment. The reaction tail gas was analyzed using GC with a packed column of 5A connected to TCD detector. The conversion of LA and the product selectivity were calculated according to equations (2) and (3).

$$t_C = \frac{3600 \times 273.15 \times V_{cat.}}{22400 \times (n_{LA} + n_{H_2O} + n_C) \times T} \quad \text{------(1)}$$

Where t_C is contact time (s), $V_{Cat.}$ is catalyst volume (mL), n_{LA} is the moles of lactic acid passed per hour, n_{H_2O} is the moles of water in lactic acid aqueous solution feed passed per hour, n_C is the moles of carrier gas (air) passed per hour and T is reaction temperature (K).

$$\text{Conversion}\ (\%) = \frac{n_0 - n_1}{n_0} \times 100 \quad \text{-----(2),} \qquad \text{Selectivity}\ (\%) = \frac{n_p}{n_0 - n_1} \times 100 \quad \text{------(3)}$$

Where n_0 is the molar quantity of LA fed into reactor, n_1 is the molar quantity of LA in the effluent, and n_p is the molar quantity of lactic acid converted to PA or other byproducts such as acetaldehyde and acrylic acid.

The rate of oxidative dehydrogenation of lactic acid was calculated assuming a pseudo-first-order reaction as below,

$$\ln(1-x) = -kC_{cat}t$$

where k is the pseudo-first-order rate constant (h^{-1}), x is the conversion of lactic acid, C_{cat} is the concentration of catalyst under reaction system and t is the reaction time (h).

Computational Details

We have performed the DFT simulations via CASTEP code to comprehend the catalytic mechanism of lactic acid adsorbed on the surface of Fe_2O_3. In this work, the GGA-PBE function[5, 6] was employed and the energy cutoff value was set to be 400 eV. A Monkhorst-Pack k-mesh[7] $7 \times 7 \times 1$ for the crystalline surface (001), (012) and (113) with vacuum layer of 15 Å added in the slab was adopted. The threshold of the general energy convergence of crystalline relaxation is 10^{-6} eV. During the relaxation of the surfaces covered with lactic acid, the top three layers and the absorbates were allowed to move, while the bottom three layers of the slab kept fixed. The Dipolar correction are also included perpendicular to the slab. The adsorption energy E_{ads} could be obtained as follows:

$$E_{ads} = E_{total} - E_{surf} - E_{absorbate},$$

where E_{total} is the total energy of lactic acid absorbate covered on a surface, E_{surf} is the energy of a surface and $E_{absorbate}$ presents the energy of free lactic acid molecule in vacuum. A negative E_{ads} indicates the stability of lactic acid absorbed on the surface thermodynamically.

Characterization

The specific surface areas of catalysts were measured by nitrogen physical adsorption at 77 K using JW-BK100C instrument. Powder X-ray diffraction measurement was carried out on a Dmax/Ultima IV diffractometer by operating at 40 kV and 20 mA with Cu-Ka radiation. Diffuse reflectance UV-Vis spectra were applied on a Shimadzu UV-2401 PC spectrometer in a diffuse-reflectance mode by using an integrating sphere (internal diameter 60 mm) and $BaSO_4$ was used as the reference. Redox properties of the samples were evaluated by H_2-TPR on a Finesorb-3010 Instrument. X-ray photoelectron spectroscopy (XPS) measurements were performed using a Thermo Scientific K-Alpha spectrometer, equipped with a monochromatic small-spot X-ray source and a 180° double focusing hemispherical analyzer with a 128-channel detector. The binding energy was corrected for surface charging by taking the C 1s peak of contaminant carbon as a reference at 284.6 eV. Particle morphology was characterized on a Hitachi S4800 field-emission scanning electron microscope (SEM). TEM and HRTEM images were obtained using a Tecnai G^2F20 U-TWIN microscope operating at 200 kV.

Results and Discussion

Effect of mass transfer during the catalytic reaction. From Fig. S1a, the effect of catalyst particle size on the oxidative dehydrogenation of LA to PA was visibly observed, that is, the LA conversion rate increases sharply with the decrease of the catalyst particle size, indicating an internal diffusion limit. With the particle size of the catalyst decreased to 20-40 mesh, the conversion rate of LA is equivalent to the catalyst of 40-60 mesh, indicating that the internal diffusion limitation can be easily eliminated. Fig. S1b shows that the LA conversion rate is stable with time on stream, and no induction period

in this reaction occurs. Subsequently, the external diffusion limitation was further investigated using 20-40 mesh sized catalysts. At a fixed LA/O_2 molar ratio and contact time, the conversion rate of LA is significantly affected by LA flow rate (Fig. S2a), indicating the existence of external diffusion restriction. As the flow rate added to 1.0 mL h^{-1} with 1.5 cm height of the catalyst, the external diffusion limitation is effectively eliminated. Similarly, LA conversion also stabilizes with time on stream (Fig. S2b). In the subsequent experiment for activity evaluation, the catalyst particle size was selected as 20-40 mesh, and the LA flow rate was selected as 2.0 with 3.0 cm height of the catalyst in a fixed bed reactor to remove the mass transfer effect.

Oxidation properties. For all α-Fe_2O_3 sample, the power X-ray diffraction (XRD) peaks (as shown in Fig. 1a) can be confirmed to a rhombohedral hexagonal phase (space group R-3C) with lattice constants a=b=0.5036 nm and c=1.3749 nm. The oxidation state of the four α-Fe_2O_3 as-prepared samples was detected by X-ray photoelectron spectroscopy (Fig. S7b). The nature of the Fe 2p peak broadening is very complicated, which is caused by the electrostatic interaction between the photoionized Fe 2p nuclear pore and unpaired Fe 3d electrons, spin-orbit coupling and crystal field interaction[8]. The centroids of Fe $2p_{3/2}$ and $2p_{1/2}$ peaks are located at 710.4 and 724.2 eV, respectively. The binding energies for Fe 2p core levels is well the same as the values reported in previous work[8]. Then, the H_2-TPR experiment was carried out to further the redox properties, and the results were shown in Fig. S7c. In the four samples, RC revealed the lowest reduction peak, centered at 385 °C, and the low reduction peaks of other samples shifted toward high temperatures, such as 459 and 485 °C, higher than that in the HS and RC, also demonstrating that a strong crystal effect in the samples, which made for a variation of redox properties. Further study on the reaction mechanism of LA oxidation dehydrogenation to PA is helpful to optimize the catalyst design and reaction parameters, obtaining better catalytic performance. In previous work[9], the lattice oxygen was utilized in the oxidative dehydrogenation of LA to PA on the FeMoO/P. In the presence of α-Fe_2O_3-THB and QC, the LA conversion and PA selectivity is especially low, agreeing with that of reaction rate constant as shown in Fig. 1a and Table 1. In contrast, for HS the LA conversion and PA selectivity is significantly improved. Likewise, for RC the conversion and PA selectivity is further improved, responding to the reaction rate constant as shown in Fig. 1a and Table 1. The above analyses reflect that the LA conversion and PA selectivity follows RC > HS > QC > THB. This order fundamentally reflects the differences in the active sites among the dominant facets of the α-Fe_2O_3 structures, with {001} > {012} > {113}.

Theoretical calculation. DFT calcuations are devoted to the study of the reaction adsorption energy of oxidative dehydrogenation of LA to PA over α-Fe_2O_3. The method of establishing the surface model of the α-Fe_2O_3 catalysts is as follows: firstly, the α-Fe_2O_3 is geometrically optimized, and the atoms of (001), (012), (113) crystal orientation are intercepted (Fig. S6a). Next, the supercell construction and the vacuum layer are added, obtaining the corresponding catalyst model. Considering the accuracy of the results and the amount of calculation, the model is set to six layers. And the lower three layers are fixed, the upper three layers are relaxed. The surface vacuum layer thickness is set to 15 Å. DFT calculations were performed to evaluate the adsorption energies of various α-Fe_2O_3 surfaces and the catalytic activities of the potential catalytic sites on α-Fe_2O_3 (001) facets (Fig. S6a). The surface adsorption of LA is an important step in the heterogeneous reaction of lactic acid over α-Fe_2O_3. Considering different adsorption surfaces, the structure of lactic acid on α-Fe_2O_3 surface was optimized, and its adsorption energy was shown in the Table S4, agreeing with that of reaction rate constant as shown in Fig. 1a and Table 1. Then, we optimized the adsorption structures of LA at different adsorption sites on the α-Fe_2O_3 (001) facets, obtaining two stable adsorption configurations 1A (Fe-O) and 1B (O-H), as shown in Fig. S6b-e. Wherein, the configurations 1A and 1B are adsorbed by LA through O atoms and H atoms with Fe atoms and O atoms on the surface with different functional groups respectively, and the structural parameters of corresponding adsorption configurations 1A are as follows: Fe-O=2.186 Å and Fe-H=2.192 Å, and its adsorption energy was shown in the Table S5 and Table S6, agreeing with that of reaction rate constant as shown in Fig. 1a and Table 1, and the forecast of

mechanism as shown in Scheme 1, in which indicated that the LA molecule is activated by Fe-OH adsorption over the α-Fe_2O_3 (001) facets.

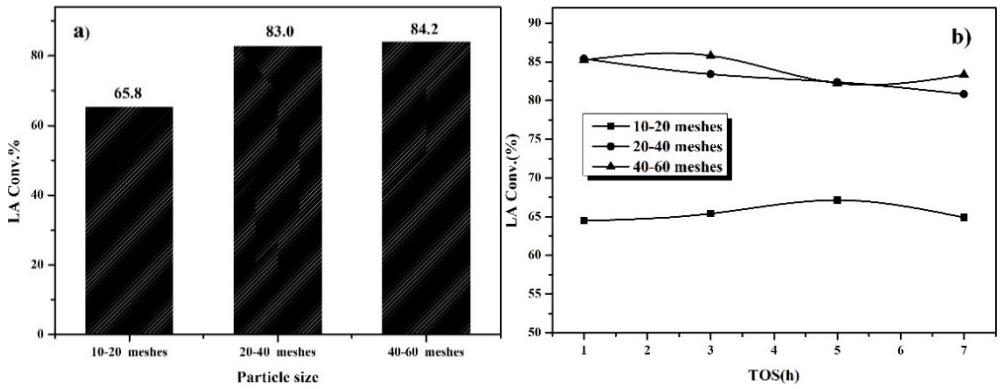

Fig. S1. Effect of catalyst particle size on the oxidative dehydrogenation of LA. Catalyst, RC, 0.38mL, the height of the catalyst bed, 3cm, 0.32-0.54g; reaction temperature 230 ^{o}C; carrier gas air, 3 mL min^{-1}; LA feedstock, feed flow rate, 2.0 g h^{-1}, LA 10 wt% in water, TOS, 1-7 h; LA, lactic acid.

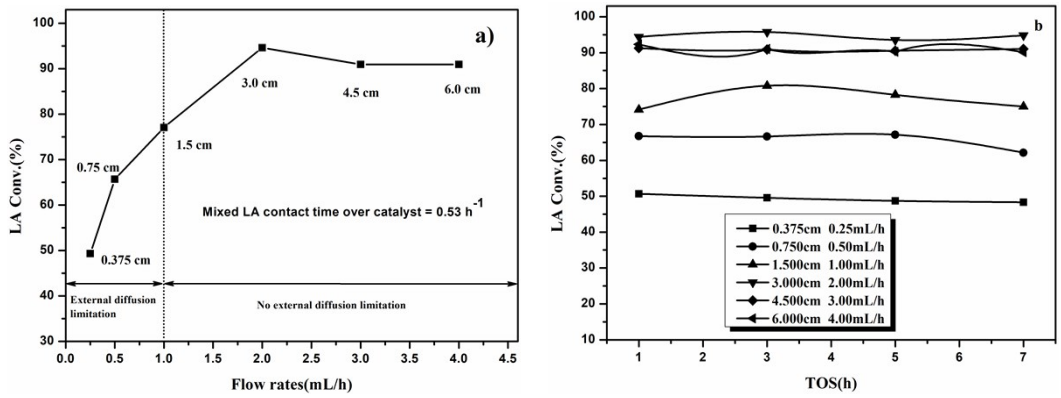

Fig. S2. Effect of LA flow rate on the oxidative dehydrogenation of LA. Catalyst, RC, 0.01-1.20 g; reaction temperature 230 ^{o}C; LA feedstock, LA 10 wt% in water, TOS, 1-7 h; LA, lactic acid.

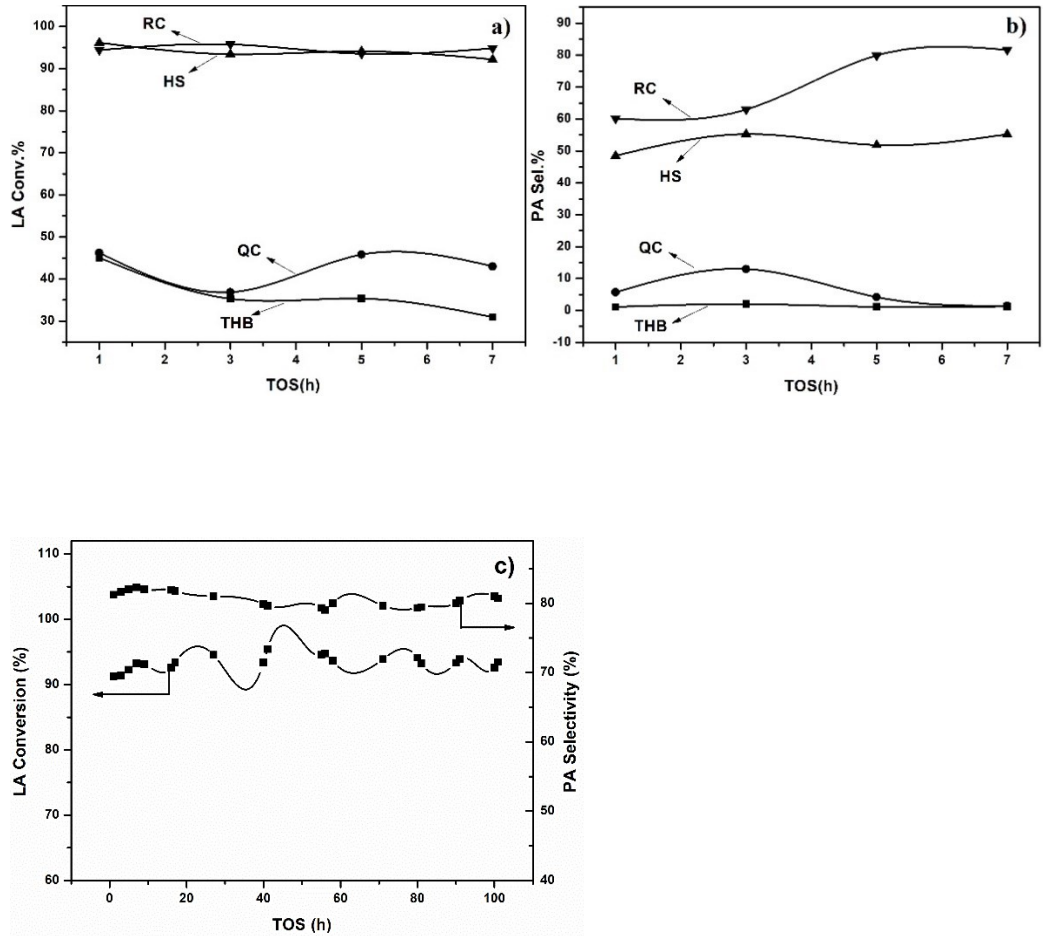

Fig. S3. Time on stream for LA conversion (a), PA selectivity (b) and the stability (c) of RC. Reaction conditions: catalyst, 0.30-0.40g; reaction temperature 230 ^{o}C; particle size, 20-40 meshes; carrier gas air, 3 mL min^{-1}; LA feedstock, 10 wt% in water, feed flow rate, 2 mL h^{-1}, TOS 1-7h.

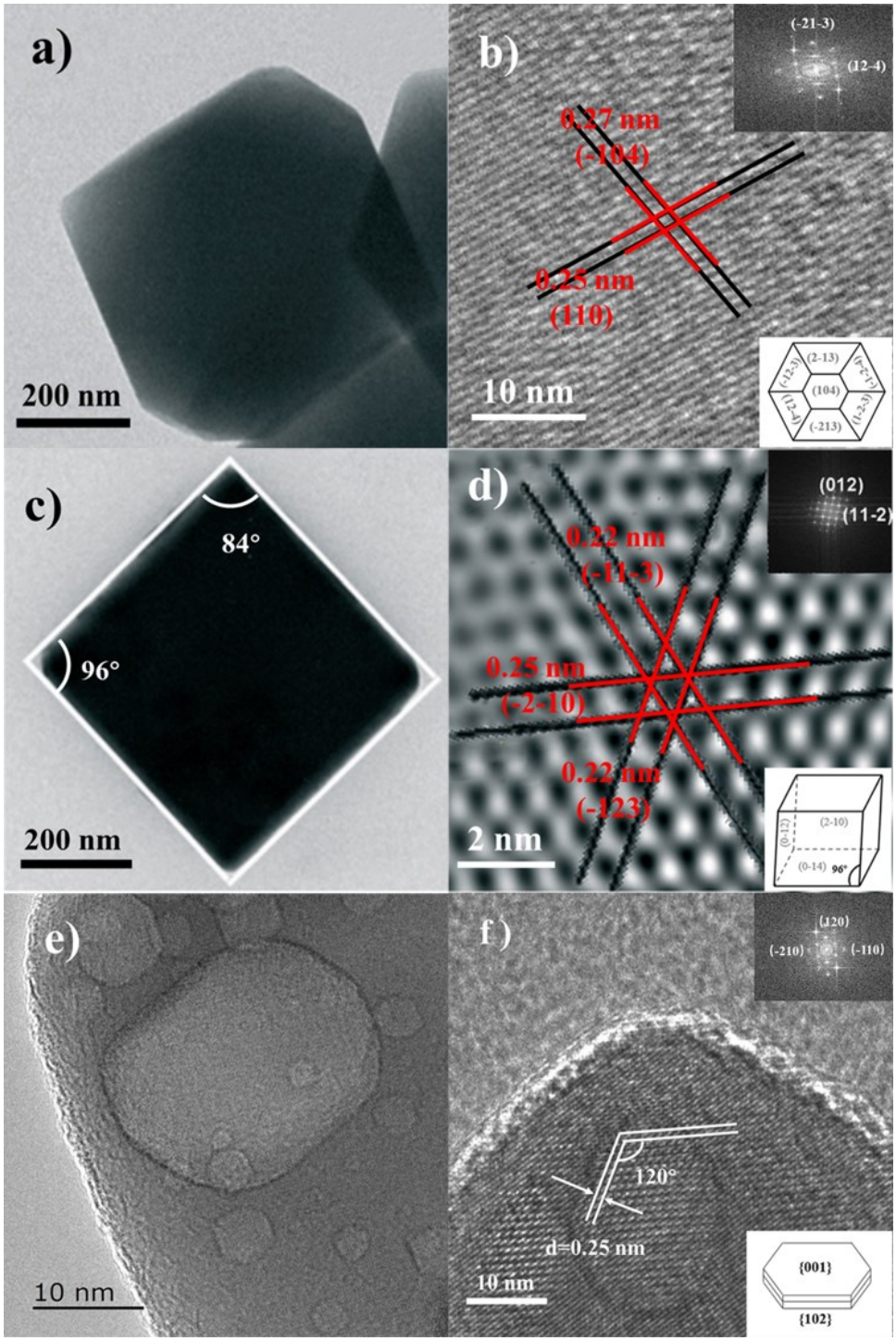

Fig. S4. Representative morphologies and structures of a-Fe_2O_3. a) TEM and b) HRTEM image of a-Fe_2O_3-THB. Insets: FFT pattern and drawing of a hexagon. c) TEM image and d) HRTEM image of a-Fe_2O_3-QC. Insets: FFT pattern and drawing of a cube. e) TEM image and f) HRTEM image of a-Fe_2O_3-HS. Insets: FFT pattern and drawing of a plate.

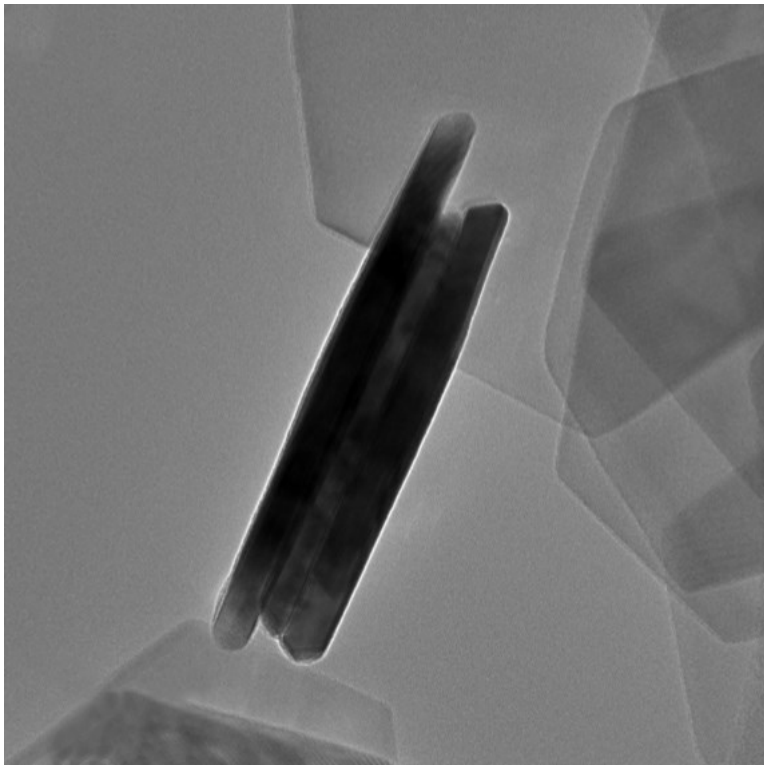

Fig. S5. Typical TEM image of the cross-section of α-Fe_2O_3 nanoplates, displaying the wedge-shaped side facets[2].

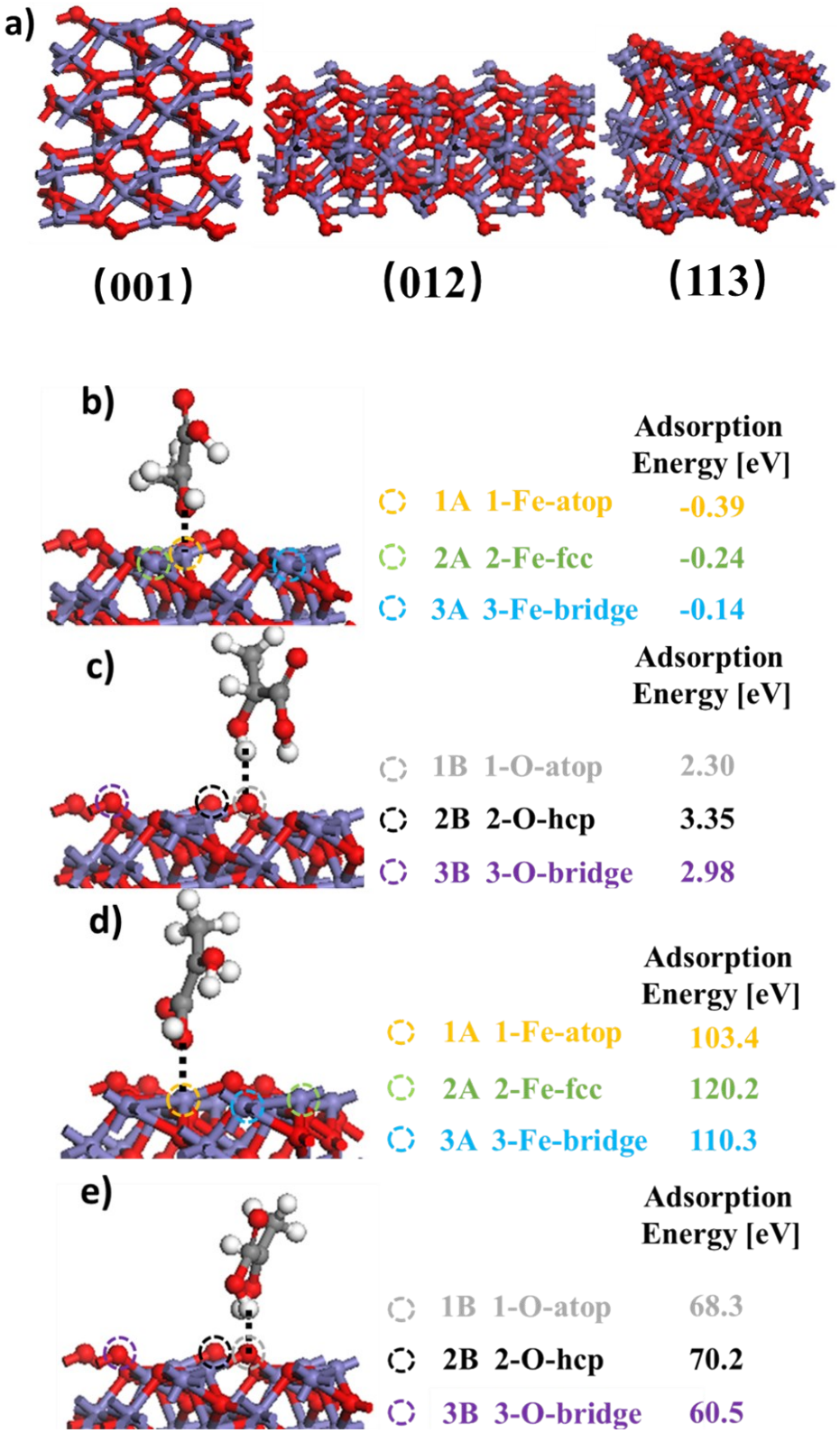

Fig. S6. (a) Surface structures of different α-Fe_2O_3 surfaces (Fe: blue, O: red). Different adsorption types of oxidative dehydrogenation of LA to PA on α-Fe_2O_3 (001) over (b) hydroxyl oxygen of lactic acid with Fe (Fe-O) over catalyst, (c) hydroxyl hydrogen of lactic acid with O (H-O) over catalyst, (d) Hydroxyl oxygen in the carboxyl group of lactic acid with Fe (Fe-O) over catalyst, (e) hydroxyl hydrogen in the carboxyl group of lactic acid with O (H-O) over catalyst. Different adsorption Fe site, namely, 1A, Fe-atop site, 2A, Fe-fcc site, 3A, Fe-bridge site and different adsorption O site, that is, 1B, O-atop site, 2B, O-hcp site, 3B, O-bridge site.

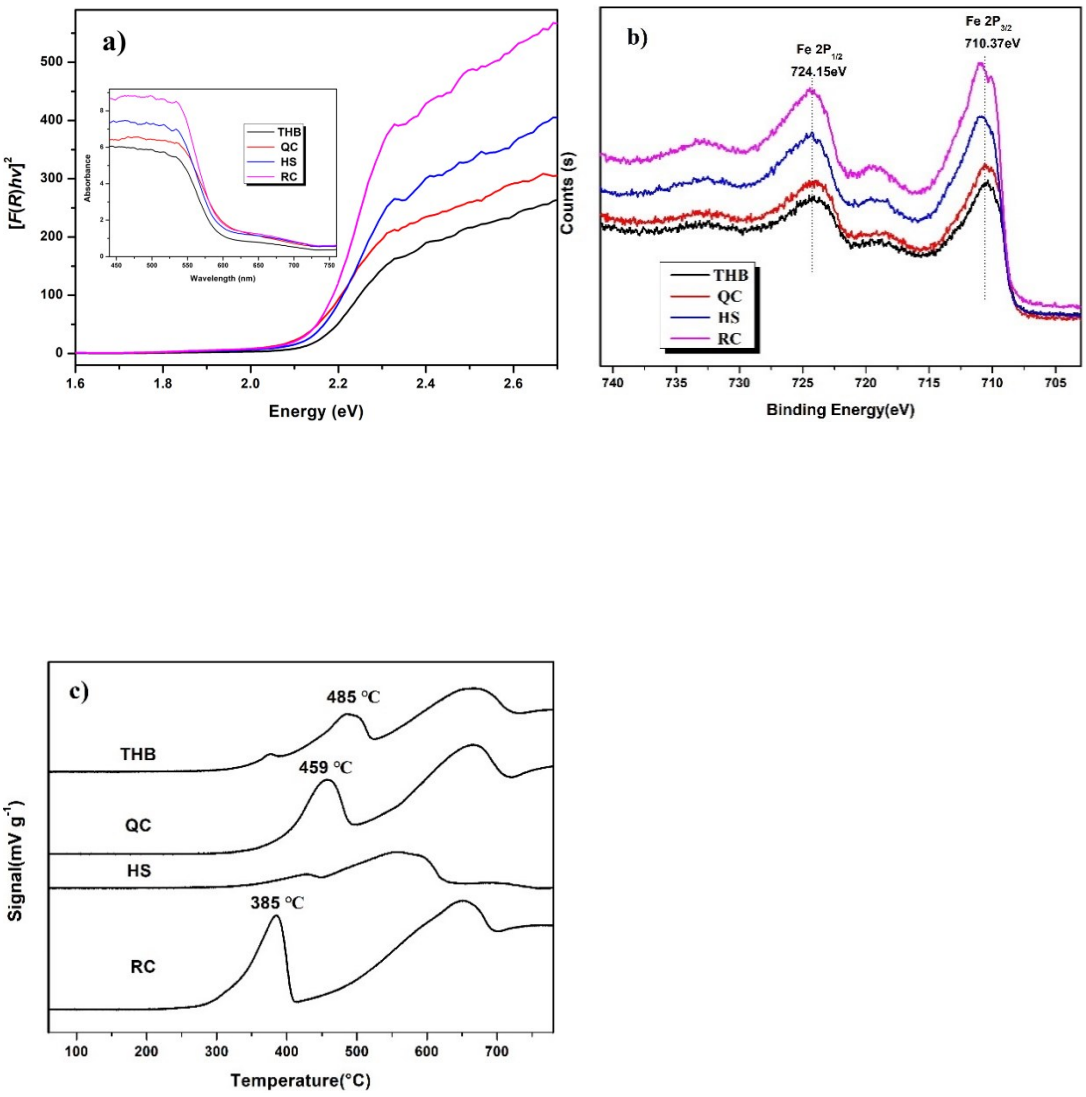

Fig. S7. (a) UV-Vis absorption spectra and corresponding Tauc plots for α-Fe_2O_3 samples. (b) XPS spectra of α-Fe_2O_3 sample (b, Fe 2p). (c) H_2-TPR profiles of α-Fe_2O_3 samples.

Table S1. Catalytic activity of α-Fe_2O_3 with different morphology for oxidative dehydrogenation of LA to PA[a].

Catalyst	L A Conv. [%]	Sel.[b] [%]				
		PA	AD	AA	ACA	Others
THB	36.7	2.1	1.4	6.1	3.2	87.2
QC	43.1	4.2	2.5	1.1	8.1	84.1
HS	94.0	55.3	8.3	16.4	10.6	9.4
RC	94.6	81.7	5.8	5.1	3.8	3.6

[a] Conditions: catalyst, 0.30-0.40g; reaction temperature 230 °C; particle size, 20-40 meshes; carrier gas air, 3 mL min^{-1}; LA feedstock, 10 wt% in water, feed flow rate, 2 mL h^{-1}, TOS on 4-5 h. [b] LA, lactic acid; PA, pyruvic acid; AD, acetaldehyde, AA, acrylic acid; ACA, acetic acid.

Table S2. The adsorption energy of oxidative dehydrogenation of LA to PA on different adsorption facets of α-Fe_2O_3.

Facet	{012}	{113}	{001}
E (eV)	10.45	10.23	-0.39

Adsorption energy calculation formula, $E_{ads}=E_{total}-E_{surf}-E_{absorbate}$, the energy of lactic acid adsorbed on α-Fe_2O_3.

Table S3. The adsorption energy of oxidative dehydrogenation of LA to PA on facets (001) of α-Fe_2O_3.

Adsorption configuration	1A	1B	2A	2B	3A	3B
E (eV)	-0.39	2.30	-0.24	3.35	-0.14	2.98

Adsorption energy calculation formula, $E_{ads}=E_{total}-E_{surf}-E_{absorbate}$, the energy of independent α-Fe_2O_3 (001); $E_{absorbate}$, the energy of lactic acid adsorb on α-Fe_2O_3 (001)-Fe-O or O-H over hydroxyl oxygen and hydrogen.

Table S4. The adsorption energy of oxidative dehydrogenation of LA to PA on facets (001) of α-Fe_2O_3.

Adsorption configuration	1A	1B	2A	2B	3A	3B
E (eV)	103.4	68.3	120.2	70.2	110.3	60.5

Adsorption energy calculation formula, $E_{ads}=E_{total}-E_{surf}-E_{absorbate}$, the energy of independent α-Fe_2O_3 (001); $E_{absorbate}$, the energy of lactic acid adsorb on α-Fe_2O_3 (001)-Fe-O or O-H over hydroxyl oxygen and hydrogen on carboxyl.

Table S5. The physical properties of four α-Fe_2O_3.

Sample	E_g (eV)	E_{VB} (eV)	E_{CB} (eV)
THB	2.13	2.455	0.325
QC	2.10	2.440	0.340
HS	2.14	2.460	0.320
RC	2.15	2.465	0.315

Table S6. Catalytic activity of THB and QC with different reaction temperature for oxidative dehydrogenation of LA to PA[a].

Reaction Temperature [°C]	L A Conv. [%]	Sel.[b] [%]				
		PA	AD	AA	ACA	Others
230 [c]	36.7	2.1	1.4	6.1	3.2	87.2
260 [c]	50.4	25.8	15.6	8.6	6.8	43.2
290 [c]	35.6	5.5	28.6	7.3	7.5	51.1
230 [d]	43.1	4.2	2.5	1.1	8.1	84.1
260 [d]	53.2	28.5	17.8	5.6	7.3	40.8
290 [d]	39.7	7.8	30.3	3.6	6.7	51.6

[a] Conditions: catalyst, 0.30-0.40g; particle size, 20-40 meshes; carrier gas air, 3 mL min^{-1}; LA feedstock, 10 wt% in water, feed flow rate, 2 mL h^{-1}, TOS on 4-5 h. [b] LA, lactic acid; PA, pyruvic acid; AD, acetaldehyde, AA, acrylic acid; ACA, acetic acid. [c] catalyst, THB. [d] catalyst, QC.

References

1 L. Gu, Q. Su, W. Jiang, Y. Yao, Y. Pang, W. Ji, C.-T. Au, *Catal. Sci. Technol.* **2018**, *8*, 5782-5793.
2 L. Chen, X. Yang, J. Chen, J. Liu, H. Wu, H. Zhan, C. Liang, M. Wu, *Inorg. Chem.* **2010**, *49*, 8411-8420.
3 Z. J. Zhai, X. L. Li, C. M. Tang, J. S. Peng, N. Jiang, W. Bai, H. J. Gao, Y. W. Liao, *Ind. Eng. Chem. Res.* **2014**, *53*, 10318-10327.
4 J. F. Zhang, J. P. Lin, P. L. Cen, *Can. J. Chem. Eng.* **2008**, *86*, 1047-1053.
5 J. P. Perdew, K. Burke, M. Ernzerhof, *Phys. Rev. Lett.* **1996**, *77*, 3865-3868.
6 R. Elmer, M. Berg, L. Carlen, B. Jakobsson, B. Noren, A. Oskarsson, G. Ericsson, J. Julien, T. F. Thorsteinsen, M. Guttormsen, G. Lovhoiden, V. Bellini, E. Grosse, C. Muntz, P. Senger, L. Westerberg, *Phys. Rev. Lett.* **1996**, *77*, 4884-4886.
7 J. D. Pack, H. J. Monkhorst, *Phys. Rev. B* **1977**, *16*, 1748-1749.
8 J. Baltrusaitis, D. M. Cwiertny, V. H. Grassian, *Phys. Chem. Chem. Phys.* **2007**, *9*, 5542-5554.
9 C. Yin, X. Li, Z. Chen, W. Zou, Y. Peng, S. Wei, C. Tang, L. Dong, *New J. Chem.* **2020**, *44*, 5884-5894.